Biophysical Journal
Article

Biophysical Society

A Loose Relationship: Incomplete H^+/Sugar Coupling in the MFS Sugar Transporter GlcP

Andre Bazzone,[1] Annas J. Zabadne,[1] Anastasia Salisowski,[2] M. Gregor Madej,[1] and Klaus Fendler[1,*]
[1]Max Planck Institute of Biophysics, Frankfurt/Main, Germany and [2]Johann Wolfgang Goethe-University, Frankfurt/Main, Germany

ABSTRACT The glucose transporter from *Staphylococcus epidermidis*, $GlcP_{Se}$, is a homolog of the human GLUT sugar transporters of the major facilitator superfamily. Together with the xylose transporter from *Escherichia coli*, $XylE_{Ec}$, the other prominent prokaryotic GLUT homolog, $GlcP_{Se}$, is equipped with a conserved proton-binding site arguing for an electrogenic transport mode. However, the electrophysiological analysis of $GlcP_{Se}$ presented here reveals important differences between the two GLUT homologs. $GlcP_{Se}$, unlike $XylE_{Ec}$, does not perform steady-state electrogenic transport at symmetrical pH conditions. Furthermore, when a pH gradient is applied, partially uncoupled transport modes can be generated. In contrast to other bacterial sugar transporters analyzed so far, in $GlcP_{Se}$ sugar binding, translocation and release are also accomplished by the deprotonated transporter. Based on these experimental results, we conclude that coupling of sugar and H^+ transport is incomplete in $GlcP_{Se}$. To verify the viability of the observed partially coupled $GlcP_{Se}$ transport modes, we propose a universal eight-state kinetic model in which any degree of coupling is realized and H^+/sugar symport represents only a specific instance. Furthermore, using sequence comparison with strictly coupled $XylE_{Ec}$ and similar sugar transporters, we identify an additional charged residue that may be essential for effective H^+/sugar symport.

INTRODUCTION

Members of the GLUT family of membrane transporters mediate sugar transport in eukaryotic cells. The 14 identified human GLUT transporters are expressed in virtually all tissues and have been related to a number of diseases (1). Most human GLUT transporters are identified as facilitative transporters or uniporters with a few exceptions: GLUT13 seems to be a H^+/myo-inositol symporter (2), and the status of GLUT12 in controversial; it has been described as being able to perform uniport (3) and/or H^+/glucose symport (4).

A prokaryotic homolog of GLUT transporters is the H^+/xylose symporter from *Escherichia coli* $XylE_{Ec}$. The coupling proton binds in $XylE_{Ec}$ to an aspartate in position 27 (D27) (5). Most GLUT transporters have an uncharged alanine or asparagine in the equivalent position (6), which obviously makes them unable to perform H^+-coupled transport, due to the missing H^+-binding site. But there are exceptions: GLUT2, 10, 12, and 13 have charged residues in analogous positions, aspartates or glutamates, which could serve as H^+-binding sites. Indeed, GLUT12 and 13 have been suggested to be H^+-coupled symporters.

Another prokaryotic glucose transporter is GlcP from *Staphylococcus epidermidis* $GlcP_{Se}$. Like $XylE_{Ec}$ and many other bacterial sugar transporters, it is a member of the major facilitator superfamily (MFS). The recently solved crystal structure in the inward-facing conformation (6) opens the way for a molecular interpretation of functional data. Although most GLUTs are facilitative transporters likely because of the easy availability of sugar in animal tissue, it has been argued that bacterial sugar transporters are H^+-coupled symporters. Accordingly, in an in vitro assay $GlcP_{Se}$ has been shown to be capable to perform $\Delta\tilde{\mu}_{H^+}$-driven sugar uptake (6). However, our electrophysiological measurements show counterintuitive results—we could not detect electrogenic steady-state glucose transport as implied by $\Delta\tilde{\mu}_{H^+}$-driven sugar uptake.

In this report we present an electrophysiological analysis of the $GlcP_{Se}$ transport activity combined with radioactive transport measurements and kinetic model calculations. Our results support the notion that $GlcP_{Se}$ is neither a strictly coupled H^+/glucose symporter nor a glucose uniporter, but a loosely coupled H^+/glucose transporter, which, depending on conditions, can show unconventional transport phenotypes.

Submitted August 1, 2017, and accepted for publication September 29, 2017.

*Correspondence: klaus.fendler@biophys.mpg.de

Editor: Ian Forster.

https://doi.org/10.1016/j.bpj.2017.09.038

The fact that some of the GLUT sugar transporters have a H^+-binding site in a conserved position but are reported as uniporters has led to the conclusion that an additional structural element is needed for symport (6). Combining sequence comparison with the functional analysis of $GlcP_{Se}$ and mutational analysis of $XylE_{Ec}$, we identify such an element in $XylE_{Ec}$, namely a conserved glutamate in position 206 that may serve as a pK switch (7). Our results shed new light on the assignment of transport function to sugar transporters, bacterial as well as eukaryotic, and may resolve the controversy regarding the transport modes of some of the GLUT transporters.

MATERIALS AND METHODS

Protein production

The plasmid pET15b with the wild-type (WT) $GlcP_{Se}$ construct was kindly provided by Jun-Yong Choe (The Chicago Medical School, Rosalind Franklin University of Medicine and Science, Chicago, IL). The D22N and I105S mutants were created by site-directed mutagenesis using the QuikChange Site-Directed Mutagenesis Kit (Stratagene, San Diego, CA).

The WT $GlcP_{Se}$ and the respective mutants were purified from *E. coli* BL21(DE3). Cells were grown in 2YT media at 37°C, followed by induction at OD_{600} 0.8 with 0.2 mM IPTG and growth was continued at 37°C for 3 h. After centrifugation (15 min, 4500 × *g* at 4°C), the cells were disrupted by a microfluidizer at 12,000 psi followed by low-speed centrifugation (15 min, 9500 × *g* at 4°C). The supernatant was used for ultracentrifugation (1 h, 100,000 × *g* at 4°C) to harvest the membranes that were frozen and stored at −80°C.

Membranes were solubilized at 5 mg/mL total protein in 50 mM sodium phosphate (NaPi, pH 7.5) containing 200 mM NaCl, 5 mM imidazole, a protease inhibitor cocktail tablet (cOmplete Tablets EDTA-free EASYpack; Roche Diagnostics, Basel, Switzerland), and 1% (w/v) n-dodecyl-β-D-maltoside (DDM) on ice. After centrifugation for 1 h (100,000 × g at 4°C), the supernatant was used for purification of the His-tagged proteins by metal affinity chromatography. After loading the sample and washing with 5 and 30 mM imidazole in 50 mM NaPi at pH 7.5 and 0.01% (w/v) DDM, purified proteins were eluted with 200 mM imidazole in the same buffer and 0.01% (w/v) DDM.

The eluted sample (10 mL) was concentrated to 2–5 mg/mL, final concentration, by using a concentrator with a 10-kDa cutoff (Amicon Ultra Centrifugal Filters Ultracel-10K; Millipore, Billerica, MA). At the same time, the buffer was exchanged with the buffer used for reconstitution (100 mM KPi, pH 7.5, 2 mM MgSO4). The concentrated sample was used directly for reconstitution.

Reconstitution of proteoliposomes

Reconstitution of purified proteins (2–5 mg/mL) was carried out with *E. coli* phospholipids (*E. coli* polar lipid extract; Avanti Polar Lipids, Alabaster, AL). Preformed liposomes (0.2–2 mL, 10 mg/mL) dissolved in 1% (w/v) octyl glucoside and the protein suspension were mixed on ice to a concentration of 0.2 mg protein/mg lipid (lipid to protein ratio (LPR) 5). The LPR 5 sample was used for all solid-supported membrane (SSM) measurements. Reconstitution for radioactive transport assays was identical, except that LPR 100 was used.

All proteins were reconstituted using overnight incubation in 400 mg/mL BioBeads (SM-2 Adsorbent Media; Bio-Rad, Hercules, CA) at 4°C. After reconstitution, the samples were diluted to 2.5 mg/mL lipid concentration, frozen in liquid nitrogen, and stored at −80°C.

SSM-based electrophysiology

SSM measurements were performed as described (8–10). After thawing the sample and sonication in a water bath (Sonorex RK 52 H; Bandelin, Berlin, Germany) for ∼30 s, 30 μL of proteoliposomes (2.5 mg/mL lipid at LPR 5) were allowed to adsorb for 1–2 h to an octadecanethiol/diphythanoyl-phosphatidylcholine hybrid bilayer on a gold surface (the sensor).

Two different solution exchange protocols were used. 1) For the measurements under symmetrical pH conditions, a single solution exchange configuration (9) was employed that consisted of three sequential phases of 0.5 s duration each: flow of nonactivating solution (NA), activating solution (A), and nonactivating solution (NA). Only the activating solution contained the sugar. 2) For the measurements under asymmetrical pH conditions, a double solution exchange configuration (9) was employed where an additional resting solution (R) phase of 2 s was added to the end of the protocol. This allowed the incubation of the sample at a different pH: an incubation time of 3–20 min depending on the pH change adjusts the inner pH of the proteoliposomes to the pH of R and establishes a pH gradient at the beginning of each subsequent measurement (7,9).

Instruments with different time resolutions were used as required. The high time-resolution setup with a valveless diverter fluidic geometry had a flow rate of ∼0.5 mL/s and a time resolution of ∼5 ms. The low time-resolution setup had a flowrate of 2 mL/s and a time resolution of ∼15 ms (11).

Currents were recorded throughout the entire time and amplified with a current amplifier set to a gain of 10^9 V/A and a rise time of 10 ms (low time-resolution setup) and 3 ms (high time-resolution setup).

All solutions were buffered in 100 mM KPi at a given pH value. The A solution contained the respective sugar at a given concentration to induce the symport reaction.

For the monensin control measurements, 10 μM monensin was added to all solutions, A, NA, and R. For equilibration, the sample was incubated in monensin containing R solution for 20 min before the measurements.

Electrophysiological data analysis and representation

When different transient currents are shown in one graph, all traces were recorded from the same sensor and the transient currents shown are representative results. Similar transient currents were observed with at least three different sensors. For substrate dependencies, the peak currents from each sensor were normalized to the respective maximum current, followed by averaging.

Currents recorded on the SSM are capacitively coupled and, therefore, intrinsically transient. However, transporter currents including steady-state components can be reconstructed using the electrical properties of the SSM/proteoliposome system (12).

Experimental determination of $K_{D,app}$ and pK_{app}

For determination of apparent K_D values, $K_{D,app}$, the concentration dependence of the normalized peak currents (I_{norm}) was fitted with a hyperbolic equation (c = sugar concentration):

$$I_{norm} = I_{max}\frac{c}{c + K_{D,app}}.$$

For determination of the apparent pK values, pK_{app}, the pH dependencies of the normalized peak integrals (Q_{norm}) were fitted using a titration function. These model functions are functions of a single H^+-binding group with pK_{app}. Q_{min} is the normalized charge at extremely alkaline pH, and Q_{max} is the charge increment obtained when going to acidic pH:

$$Q_{norm}(pH) = \frac{Q_{max}}{1 + 10^{pH - pK_{app}}} + Q_{min}.$$

Radioactive transport assays

Purified protein was used for reconstitution with 10 mg/mL *E. coli* polar lipid extract (Avanti Polar Lipids) in 100 mM KPi (pH 7.5) to yield a LPR of 100 (see above). To adjust the pH, 100 μL of the sample is mixed with 1.5 mL KPi of the respective pH (5.5 or 9.5). After ultracentrifugation for 30 min (100,000 $\times$ *g*), proteoliposomes are resuspended in 100 μL KPi of the respective pH and sonicated in a water bath for 30 s.

For the counterflow assay, the proteoliposomes were preloaded with 20 mM nonlabeled D-glucose by sonication in a water bath for ~3 min. A quantity of 5 μM ^{14}C labeled D-glucose (NEC042X050UC, 250–360 mCi/mmol; Perkin Elmer, Waltham, MA) was added to the external buffer. For the exchange assay, proteoliposomes were preloaded with 50 μM ^{14}C labeled D-glucose and the buffer contained the same concentration of nonlabeled D-glucose.

Both radioactive transport assays were started by addition of 100 μL external buffer to 2 μL preloaded proteoliposomes of the same pH. The reaction was stopped after 3 s to 30 min by addition of 1 mL ice-cold quenching buffer (100 mM KPi, pH 5.5, 100 mM LiCl) after vacuum filtration through a 200-nm polycarbonate filter. After washing the filter once with 3 mL quenching buffer, the filter was placed in scintillation tubes and 5 mL BioSafe II scintillation solution (Research Products International, Prospect, IL) was added. The radioactivity was measured after incubation for 24 h.

The background was measured at $t = 0$ s by simultaneous addition of 100 μL external buffer and quenching buffer to 2 μL proteoliposomes. As a control, proteoliposomes containing $XylE_{Ec}$ at the same LPR and at pH 5.5 were used.

Model calculations

Transport was simulated based on an eight-state kinetic model. The transport activity was determined from an analytical solution of the kinetic equations using the computer-algebraic software Mathcad (Parametric Technology, Needham, MA). For details, see the Supporting Material.

RESULTS

Transient currents after sugar concentration jumps

Proteoliposomes containing the reconstituted sugar transporter $GlcP_{Se}$ were characterized by SSM-based electrophysiology. Sugar concentration jumps initiate a charge transfer, which is measured through capacitive coupling (9). The recorded transient currents monitor steady-state or pre-steady-state charge displacements generated during the reaction cycle of the sugar transporter (13). In cases when the sugar induces continuous turnover of the complete transport cycle (steady-state charge displacements), the electrogenic transport process charges the membranes (the SSM and the membranes of the proteoliposomes), which leads to a progressive decrease of the observed current. The currents are, therefore, always transient. However, the peak currents correlate very well with the steady-state turnover rates (9). For electrogenic pre-steady-state reactions (14), the displaced charge (integral of transient currents) or the peak currents may be used alternatively for analysis. Because of the much lower transported charge, membrane charging may be here neglected.

D-glucose concentration jumps reveal fast transient currents with positive amplitude at acidic pH and negative amplitude at alkaline pH (Fig. 1 *a*) decaying with time constants of 3–9 ms, characteristic for pre-steady-state reactions. For comparison, a transient current recorded for a transporter performing steady-state charge translocation, the xylose/H^+ symporter from *E. coli*, $XylE_{Ec}$ (7), is included in the figure. The pH conditions were symmetrical, i.e., the pH inside and outside the proteoliposomes was the same. It is obvious that the transient current generated by $XylE_{Ec}$ decays with a much slower time constant typical for steady-state transport (compare the decay time constant of $LacY_{Ec}$ of ~27 ms (13)).

To further confirm whether the recorded transient currents represent steady-state or pre-steady-state reactions, we reconstituted WT $GlcP_{Se}$ in proteoliposomes with different LPRs. It was shown that the decay times of the transient currents decrease with lower LPR (higher protein density) for steady-state reactions due to the charging of

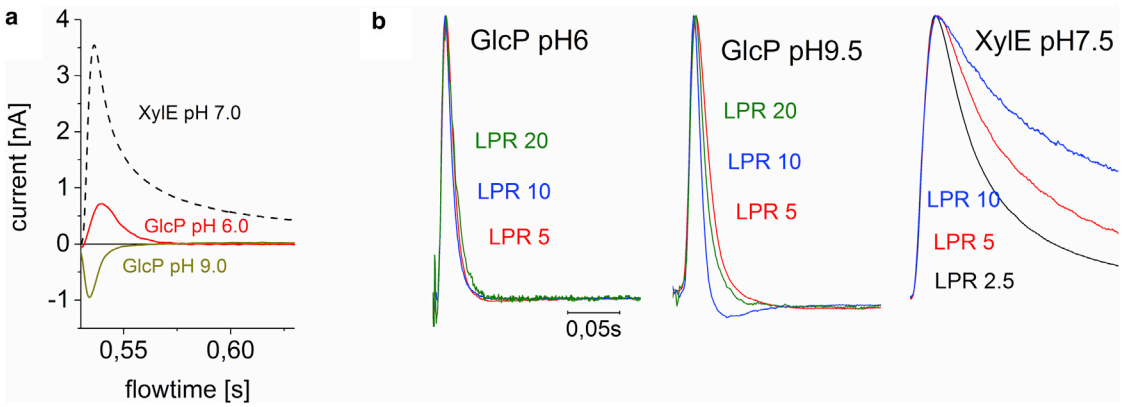

FIGURE 1 Transient currents recorded at the SSM after a substrate concentration jump at symmetrical pH as indicated. (*a*) Transient currents were generated using proteoliposomes reconstituted with WT $GlcP_{Se}$ after a 30 mM D-glucose concentration jump. For comparison, a transient current generated by $XylE_{Ec}$ using 30 mM D-xylose was included (*dashed line*). (*b*) Given here are normalized transient currents from $GlcP_{Se}$ and $XylE_{Ec}$ using liposomes reconstituted with different lipid to protein ratios, LPR (pH as indicated). The currents were normalized to their peak values to allow comparison of the current decay. The currents were recorded using the high time-resolution instrument. To see this figure in color, go online.

the membrane and consequent inhibition of the transport reaction (13). Accordingly, we observed no significant influence of LPR on the decay time (Fig. 1 *b*) of the $GlcP_{Se}$ currents, whereas the currents generated by $XylE_{Ec}$ decay faster at lower LPR, corresponding to higher protein density (Fig. 1 *b*). In conclusion, the currents recorded with $GlcP_{Se}$ show all the characteristics of an electrogenic pre-steady-state reaction and do not represent continuous turnover. In fact, sugar-induced pre-steady-state charge displacements are common among MFS proton-coupled sugar transporters $LacY_{Ec}$, $FucP_{Ec}$, and $XylE_{Ec}$, and some of their variants (7,14,15).

pH dependence of transient currents

The pH dependence of the transient currents generated by WT $GlcP_{Se}$ after a sugar concentration jump shows an atypical behavior different from other sugar transporters investigated so far (7): positive polarity at acidic and negative polarity at alkaline pH (Fig. 1 *a*). However, the behavior is complex: the transient currents decay somewhat slower at acidic pH (~9 ms) than at alkaline pH (~3 ms), giving rise to a biphasic signal at intermediate pH (see pH 8.5 in Fig. 2 *a*). This is difficult to analyze in terms of amplitudes. Therefore, we have chosen to plot the integrated transient current, which, for a pre-steady-state reaction, is proportional to the translocated charge. The normalized charge at different pH is shown in Fig. 2 *a*, together with a fit of a titration curve with a pK_{app} of 8.6.

A similar pH dependence is observed for the variant I105S $GlcP_{Se}$ (Fig. 2 *b*). This variant is analogous to the eukaryotic glucose uniporter GLUT2 (1) and has been qualified as a functional model of a uniporting GLUT transporter (6). The rapidly decaying currents indicate a faster sugar-induced reaction than observed with the WT. The time dependence of these currents is limited by the solution exchange at the surface of the SSM (5 ms). implying a rate of $>300\ s^{-1}$ for the binding process. The pK of the reaction is nearly identical to that of the WT.

The pH dependence of transient currents recorded with the neutral replacement variant D22N $GlcP_{Se}$ is shown in Fig. 2 *c*. Here the aspartate in the putative H^+-binding site has been replaced by a neutral asparagine residue. The currents are constant throughout the whole pH range from pH 4.5 to 9.5, indicating that the protonation of the H^+-binding site is responsible for the polarity change observed in WT and I105S $GlcP_{Se}$. The data were recorded with the low time-resolution instrument, which explains the somewhat slower time dependence of the transient currents.

The transient current is a convenient monitor of the protonation state of Asp^{22}

An important clue for the origin of the current's polarity change observed at different pH comes from the analysis of the D22N variant (Fig. 2 *c*). The glutamate at position 22 has been identified as the proton-binding site (5,6). A neutral replacement of the negatively charged Asp^{22} leads to positive charge displacements over the entire pH range from pH 4.5 to 9.5 (Fig. 2 *c*), suggesting that the polarity change of the WT reflects the protonation state of Asp^{22}. We derive a pK of 8.6 from these measurements. This conclusion is consistent with the pH dependence of the I105S variant which, although unable to mediate $\Delta\tilde{\mu}_{H^+}$-driven uptake (6), like the WT has a protonatable Asp^{22} and consequently behaves like WT in the electrical measurements (Fig. 2 *b*).

Pre-steady-state currents observed in related MFS sugar transporters from *E. coli* have only positive amplitudes and are not related with a proton transfer reaction, as shown with electrophysiological experiments in deuterium oxide for $LacY_{Ec}$ (15) and $XylE_{Ec}$ (7) variants, but instead represent a sugar-induced displacement of charges localized on the protein (14,16). In $GlcP_{Se}$, however, H^+ ions are obviously involved leading to a polarity change of the currents with protonation of Asp^{22}. Consequently, the observed currents after a sugar concentration jump can serve as a convenient monitor for the protonation state of its H^+-binding site Asp^{22}.

Sugar-dependent transient currents: sugar affinity and specificity at acidic and alkaline pH

Apparent K_D values, $K_{D,app}$, were obtained by analyzing the peak currents for different sugar concentrations at pH 5.5 and 10 (Fig. 3, *a–c*). Surprisingly, and in contrast to $LacY_{Ec}$, $XylE_{Ec}$, and $FucP_{Ec}$, the sugar affinity increases significantly at alkaline pH, indicating that proton binding is no prerequisite for sugar binding. This represents essentially a negative cooperativity. The observed $K_{D,app}$ values for sugar binding to $GlcP_{Se}$ are 2.6 mM at pH 10 and 12.3 mM at pH 5.5 (Fig. 3 *c*) and up to two orders-of-magnitude higher than the K_M values observed for $GlcP_{Se}$-mediated sugar transport (30 μM (6)). The reason for this is probably a rate-limiting step after electrogenic sugar binding, which results in steady-state transport being saturated at lower concentrations than sugar binding. In addition, the transport measurements were performed in the presence of $\Delta\tilde{\mu}_{H^+}$, whereas the electrophysiological experiments were performed with a D-glucose gradient, which very likely affects the rates in the transport cycle.

In addition to D-glucose, 2-desoxy-D-glucose as well as 6-desoxy-D-glucose induce transient currents at pH 10 (Fig. 3 *d*), but not at pH 5.5. Apparent substrate specificity seems to be significantly higher at alkaline pH. To exclude the effect of the generally higher sugar affinity at alkaline pH, sugar specificity was determined at acidic pH using four-times higher sugar concentrations. Taken together, these experiments show that H^+ binding to the

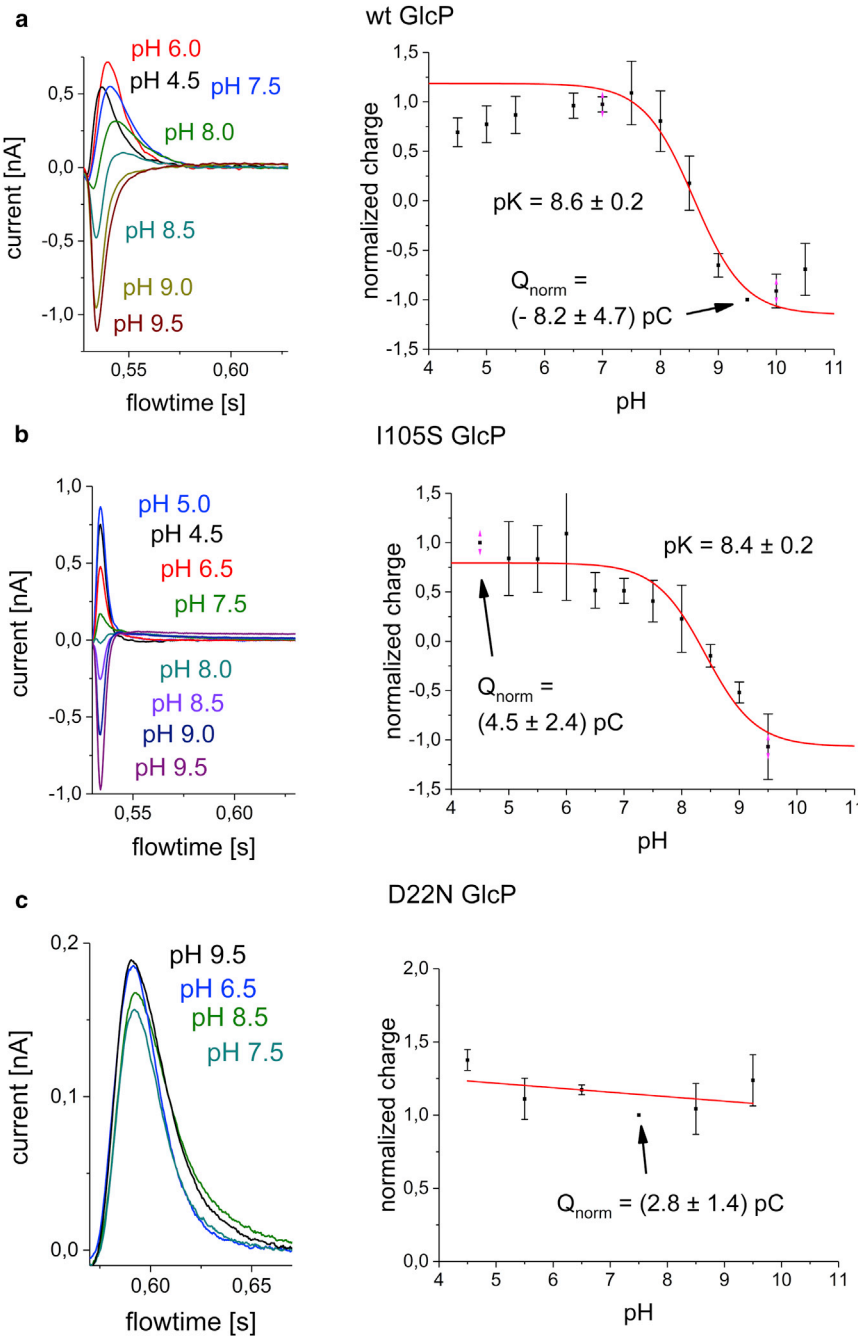

FIGURE 2 pH dependence in WT, D22N, and I105S $GlcP_{Se}$ at symmetrical pH as indicated. (*Left*) Transient currents were induced by 30 mM D-glucose at different pH values, as indicated. (*Right*) Mean and SD of the respective charge translocations (peak integrals) from at least three datasets. The data point that was normalized to 1 or −1 is indicated by an arrow. (*a*) WT $GlcP_{Se}$ is only slightly dependent on pH below pH 7.5 and above pH 9.5, but shows in-between a decrease in the translocated charge with a pK_{app} of 8.6 and a change in polarity. (*b*) I105S $GlcP_{Se}$ behaves similar to WT $GlcP_{Se}$ and shows with pK_{app} 8.4 almost the same pK_{app}. The decay times of the transients are in contrast to WT $GlcP_{Se}$ for I105S $GlcP_{Se}$ limited by the time resolution of the setup. (*c*) The charges translocated by D22N $GlcP_{Se}$ are independent of pH from pH 4.5 to pH 9.5, and always show positive amplitudes. Currents in (*c*) show different time dependence because they were recorded with the low time-resolution instrument while recordings in (*a*) and (*b*) were taken with the high time-resolution instrument. To see this figure in color, go online.

proton-binding site matters, and affects sugar binding to a certain extent, but is not a prerequisite for sugar binding in $GlcP_{Se}$.

Transient currents in the presence of a pH gradient

$GlcP_{Se}$ has previously been shown to be a proton-coupled symporter (6), whereas no steady-state charge transport was observed in our SSM measurements. SSM experiments in the presence of a pH gradient resolved the apparent contradiction. Previous transport measurements were performed at conditions mimicking the in vivo situation, namely in the presence of a membrane potential and a favorable pH gradient (6). We, therefore, investigated sugar-induced currents in the presence of pH gradients.

The rapid solution exchange at the surface of the SSM (5–15 ms) allows the application of a pH gradient using the double solution exchange protocol described in Materials and Methods. For this purpose, the SSM is incubated

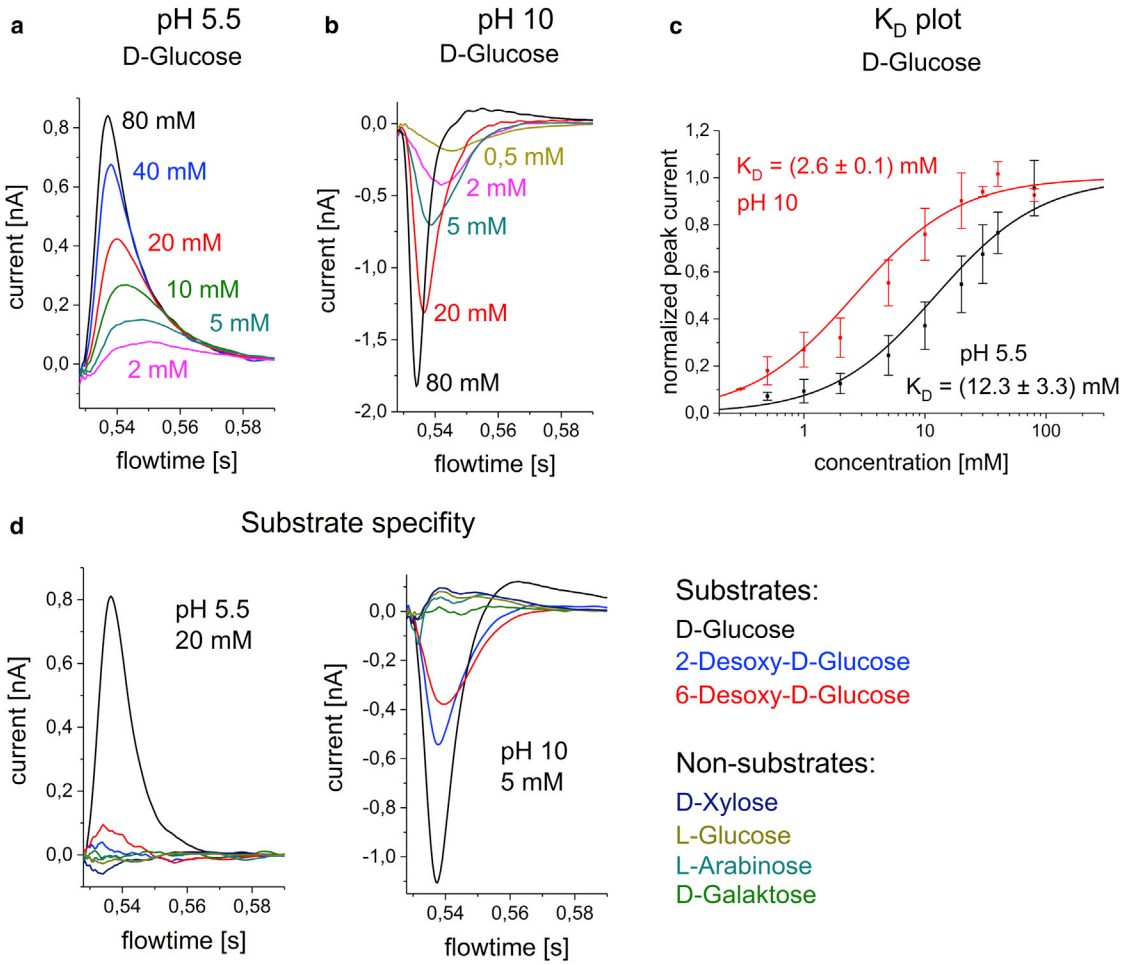

FIGURE 3 Substrate dependence at symmetrical pH as indicated. Sugar-induced currents were obtained with WT $GlcP_{Se}$ at pH 5.5 and pH 10 using the high time-resolution setup. (*a* and *b*) Transient currents induced by different D-glucose concentrations are as indicated for (*a*) pH 5.5 and (*b*) pH 10. (*c*) Plot of the averaged, normalized peak currents and SD (calculated from at least three data sets) induced by different D-glucose concentrations for pH 5.5 (*black*) and pH 10 (*red*). The hyperbolic fit reveals the apparent KD values as indicated. (*d*) Transient currents induced by different substrates (see color code) at pH 5.5 (*left*) as well as pH 10 (*right*) using sugar concentrations as indicated. To see this figure in color, go online.

in the so-called resting solution at a given pH until the pH in the liposomes has adjusted to the outer pH. Then the standard sugar concentration jump protocol is performed at a different pH establishing a pH gradient before transport is initiated by addition of the sugar substrate. For the measurements shown in Fig. 4, the resting solution was at pH 10 and the solution during the sugar concentration jump protocol was at pH 5, and vice versa—establishing pH gradients of ± 5 pH units, as shown in a schematic way in the figure.

As discussed above, currents recorded using SSM-based electrophysiology are capacitively coupled and therefore transient, even if steady-state transport activity is observed (9). However, currents of steady-state processes generally decay slower (Fig. 1). In addition, circuit analysis may be used to discriminate steady-state and pre-steady-state transport activity by reconstruction of the transporter currents. Electrically, the compound membrane formed by the planar membrane (SSM) and the adsorbed proteoliposomes are described by a characteristic time constant, the system time constant, which is a function of the involved capacitances and conductances (17). Because this time constant can be determined from the decay of the transient currents, the charging behavior of the compound membrane system can be calculated, allowing reconstruction of the transporter current from the measured current (18,19).

Fig. 4 shows the recorded transient currents (Fig. 4 *a*) together with reconstructed transporter currents (Fig. 4 *b*) in the presence and absence of pH gradients. In addition, a control measurement using the electroneutral H^+/K^+ exchanger monensin is included. In the presence of monensin, the pH gradient dissipates very fast. Therefore, monensin control currents and currents in the absence of the pH gradient are nearly identical, corroborating that the changes observed at pH gradient conditions are a direct consequence of the presence of the gradient. The left panels of Fig. 4 shows sugar-induced transient currents in the absence and presence of a pH gradient energetically favorable for H^+/sugar symport. The experimental situation is graphically

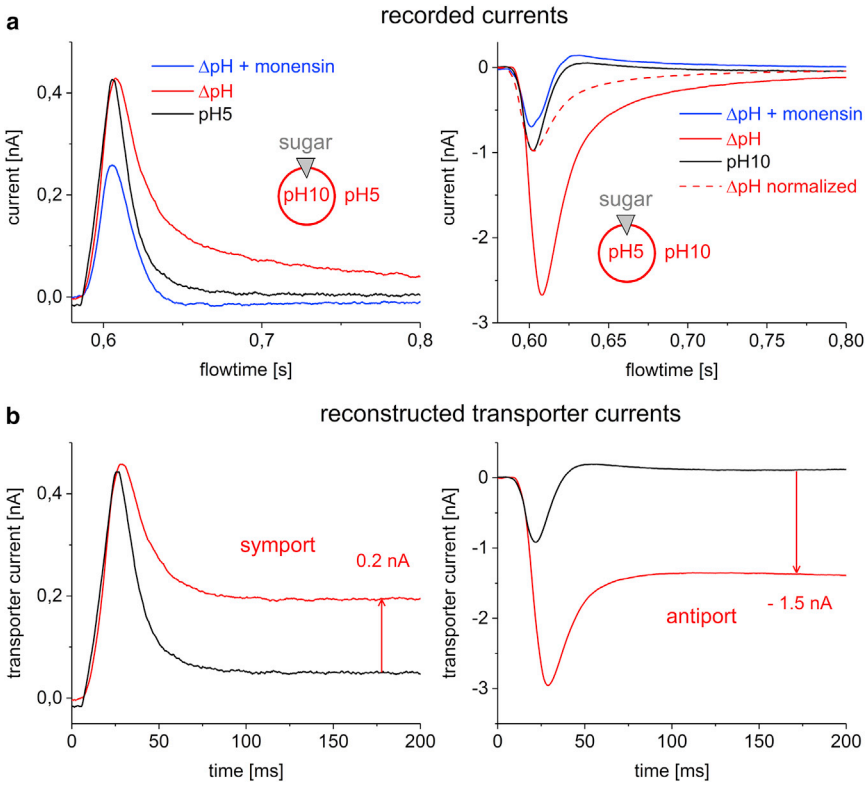

FIGURE 4 Transient currents in the absence and presence of a pH gradient. Currents recorded after a 30 mM D-glucose concentration jump using the low time-resolution instrument at symmetrical and asymmetrical pH as indicated. Transient currents shown are representative results that were reproduced on at least three different sensors. (*a*) Currents were recorded after a D-Glucose concentration jump of 30 mM in the presence (ΔpH) and absence of a pH gradient as illustrated in the figure (*gray triangle* represents the driving sugar gradient). Control currents were recorded in the absence of a pH gradient (pH5 and pH10, inside pH = outside pH) and in the presence of a gradient and 5 μM of the Na^+/H^+ exchanger monensin (ΔpH + monensin). For comparison, the peak current observed in the presence of a pH gradient was normalized to the peak current in the absence of a pH gradient (*dashed line* in the *right panel*). (*b*) Reconstructed transporter currents were determined from recorded currents in (*a*); see Materials and Methods. Color-coding is the same as in (*a*). To see this figure in color, go online.

illustrated in Fig. 4 *a*: in addition to a driving sugar gradient, a driving pH gradient is applied over the liposomal membrane using a double-solution exchange protocol. The pH indicated in the graph is that of the two subsequent solutions used to generate the pH gradient. Because pH gradients over lipid membranes dissipate rapidly, the real pH gradient may be somewhat smaller at the time of the current recording. Nevertheless, a clear effect of the gradient is observed in Fig. 4 *a*: the transient current decays considerably slower, indicating a steady-state transport process. This is illustrated by the reconstruction of the current in Fig. 4 *b* which, after a transient charge displacement, shows a clear positive steady-state current component. Positive currents represent transport of positive charge into the proteoliposomes, that is, in the same direction as sugar transport after a sugar concentration jump. The transient currents are positive, indicating that the acidic pH outside the liposome is relevant for the observed process (compare pH dependence in Fig. 2).

An analogous measurement employing a pH gradient energetically unfavorable for H^+/sugar symport is shown in the right panels of the figure. Here, the current in the presence of the gradient not only decays slower, but is also >2× larger than in its absence. The reason why the currents are larger than in the absence of a gradient and also larger than in the presence of an energetically favorable gradient is unclear, and may be related to a possible asymmetry of the transporter. To compare the time dependence of the currents in the absence and presence of the pH gradient, a normalized current trace was included (*red dashed line* in Fig. 4 *a*). Again, the current in the presence of the pH gradient decays much slower than in its absence and the reconstructed transporter current has a clear steady-state component. This indicates a steady-state transport process representing, in this case, transport of positive charge out of the proteoliposomes. The transient currents are negative, in agreement with the finding that the alkaline pH outside the liposome is relevant for the observed process (see Fig. 2).

In all experiments shown in Fig. 4, the currents are initiated by sugar addition to the outside of the proteoliposomes. Therefore, the sugar-induced process is the uptake of sugar. However, steady-state transport of positive charge depends on the applied pH gradient, and can be opposite to sugar transport. Interpreting the steady-state currents as H^+ transport suggests H^+ and sugar are transported in the same direction in the presence of an inward-directed H^+ ion concentration gradient, and H^+ and sugar are transported in opposite directions in the presence of an outward-directed H^+ ion concentration gradient.

Sugar exchange and counterflow experiments

Because charge translocation is detected at extremely acidic and alkaline pH, although with opposite polarity, it was interesting to test sugar transport at the same conditions

(Fig. 5). Therefore, exchange and counterflow experiments were performed at pH 5.5 and 9.5. Exchange measurements selectively test the sugar translocation pathways $C_oS \leftrightarrow C_iS$ (step *m*) and $H^+C_oS \leftrightarrow H^+C_iS$ (step *k*) shown in the kinetic model of Fig. 6. Counterflow measurements, in contrast, reflect the interplay of exchange and efflux: high counterflow amplitudes are indicative for high exchange and low efflux, low amplitudes for low exchange and high efflux. Therefore, counterflow experiments depend on sugar translocation (see above) but also on the velocity of the return of the sugar unloaded or apo transporter, i.e., the reactions $H^+C_i \leftrightarrow H^+C_o$ (step *n*) and $C_i \leftrightarrow C_o$ (step *j*) of the kinetic model of Fig. 6.

The time course of sugar exchange is shown in the left panel of Fig. 5 *a*. A control with liposomes reconstituted with $XylE_{Ec}$, which is known not to transport D-glucose, is included. Release of radioactively labeled sugar was linear from 0 to 32 s. In this time range, triplicate measurements were taken and linear regression yielded exchange rates that are plotted in the right panel of Fig. 5 *a*. Exchange rates at extremely acidic and alkaline pH were found to be identical. A flat pH dependence of the exchange rate was also reported for $LacY_{Ec}$ (20). However, the pK_{app} of H^+ binding in $LacY_{Ec}$ is extremely high (~10.5 (21)), leading to a protonated transporter over the whole pH range whereas, as mentioned before, the pK_{app} for H^+ binding is ~8.6 in $GlcP_{Se}$. These measurements, therefore, demonstrate that sugar translocation is independent of the occupation of the H^+-binding site.

Counterflow measurements (Fig. 5 *b*) show a high activity at acidic and a low activity at alkaline pH. This agrees with previously presented data (6). Combined with the pH-independent exchange rates determined above, this indicates that efflux is faster at alkaline pH. In the framework of our kinetic model (Fig. 6), this suggests that protonation inhibits the return of the apo transporter, which is intuitively beneficial for an H^+-coupled sugar symporter.

DISCUSSION

A universal eight-state kinetic model for symport, antiport, and uniport

Secondary active sugar symport is conventionally described by a six-state kinetic model (21) comprising ordered sugar and H^+ binding and release reactions and two conformational transitions that reorient the substrate-binding sites of the fully loaded (sugar and H^+) and the apo transporter from the extracellular to the intracellular side. Interestingly, this model can be regarded as a special case of a more general model, as shown in Fig. 6. Like in the six-state model, the transporter exists in two conformations, outward-facing (C_o) and inward-facing (C_i), and the two substrates, H^+ and sugar (S), can bind in arbitrary order to both conformations, resulting in a total of eight states. These can pairwise interconvert to their corresponding counterparts via reversible conformational transitions with the rate constants *j*, *k*, *m*, and *n*. For simplicity, substrate binding is treated as an equilibrium reaction and substrate-binding properties of the outward-facing and the inward-facing conformations are assumed to be the same. Furthermore, the forward and reverse rate constants of the conformational transition are assumed to be identical, resulting in a completely symmetrical model, which has the advantage of fulfilling automatically the principle of detailed balance. This model may be considered as a universal transporter model because it allows realization of different transporter modes found in nature: uniport, symport, and antiport. It is essentially a velocity-type transport mechanism, as already proposed in the early 1970s by Heinz and co-workers (22,23).

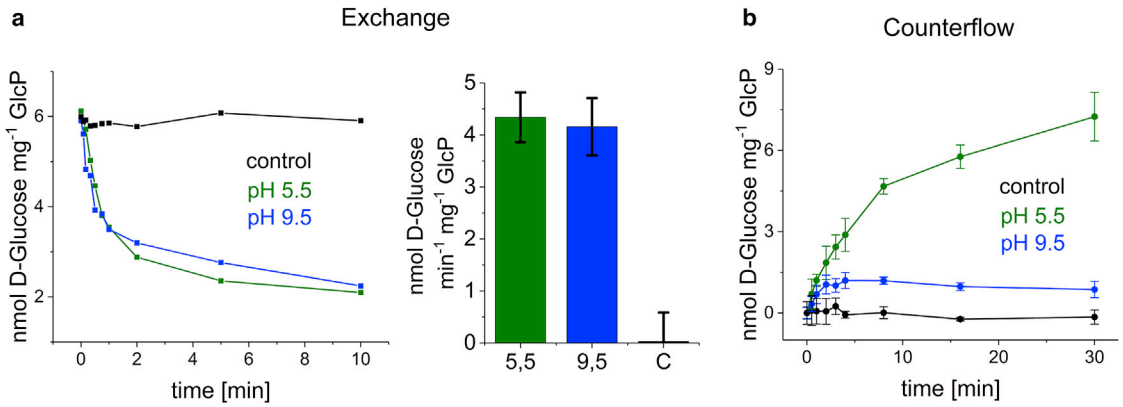

FIGURE 5 Radioactive exchange and counterflow assays. Experiments were performed using proteoliposomes containing WT $GlcP_{Se}$ equilibrated at pH 5.5 and 9.5, respectively. Control measurements were carried out using proteoliposomes containing $XylE_{Ec}$. (*a*) For the exchange assay, proteoliposomes preloaded with 50 μM ^{14}C-labeled D-glucose were incubated for different time intervals in buffer containing the same concentration of unlabeled D-glucose. The bar plot shows the mean and SD of the initial slopes derived from a linear regression of five data points from 0 to 32 s determined in triplicates. (*b*) For the counterflow assay, proteoliposomes were preloaded with 20 mM unlabeled D-glucose and suspended in buffer with 5 μM radioactive D-glucose. To see this figure in color, go online.

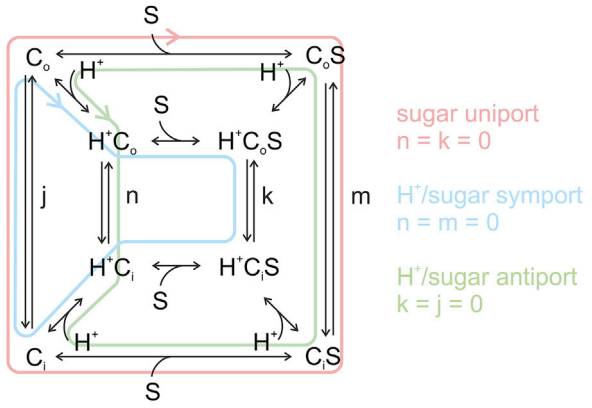

FIGURE 6 Universal eight-state kinetic model for uniport, symport, and antiport. Different transport modes—uniport, symport, and antiport—are obtained by an appropriate choice of rate constants as given in the figure. Substrate and H^+ binding are treated as rapid equilibrium reactions; forward and reverse rate constants of the conformational transitions are assumed to be identical. Model calculations of Fig. 8 are based on this kinetic model. To see this figure in color, go online.

The key to the different transport modes in the universal model are specific selection rules for the conformational transitions. H^+/sugar symport, for example, requires that the transitions between the H^+-bound ($H^+C_o \leftrightarrow H^+C_i$) and the sugar-bound conformations ($C_oS \leftrightarrow C_iS$) are not allowed, or, in other words that rate constants $n = m = 0$ (Fig. 6). Indeed, this transforms the universal model to the familiar six-state model for H^+/sugar symport. Furthermore, sugar uniport is realized if $k = n = 0$ and antiport if $k = j = 0$.

Note that the examples shown in the figure are extreme cases. The advantage of this model is that it not only allows description of perfectly coupled transport modes like uniport, symport, and antiport, but also that, by an appropriate choice of rate constants, intermediate situations like a loosely coupled transport system may be realized. We will take advantage of this property for the analysis of $GlcP_{Se}$, which shows clear indications of loose coupling.

In fact, a real transporter is very likely not an ideally coupled system. Mechanistic randomness in secondary active transport has been reported before (24). In reality, it suffices that the forbidden transitions are slow compared to the allowed transitions or that the conditions are such that the forbidden transitions are not favored. For example, it has been argued that in EmrE, a H^+-coupled multidrug exchanger, the concentration of the deprotonated carrier forms is so low that the transition between these forms (which would compromise exchange), albeit allowed, does not take place (25). It is clear that the forbidden transitions for a specific transport mode not only affect coupling but also represent leak pathways. These may result in energy dissipation and possibly have a detrimental impact on the organism.

Sugar is bound, translocated, and released by the protonated and the deprotonated transporter

As shown above (see Results), the pH-dependent pre-steady-state currents generated by $GlcP_{Se}$ reflect the protonation state of the H^+-binding site Asp^{22}. This is illustrated by the kinetic model shown in Fig. 7. It has been taken into account that many MFS sugar transporters show a rapid positive transient current upon a sugar concentration jump due to a displacement of charges fixed on the protein (14). It is best observed in the "neutral replacement mutants" (5,6,26,27), as, for example, in D22N $GlcP_{Se}$ (Fig. 2 *c*). In the model, we represent this charge displacement by a sugar binding-induced movement of a hypothetical positive charge of $\sim +0.5$ elementary charges. (This charge is hypothetical in the sense that we represent a collective electrogenic conformational transition by the displacement of a single point charge with a value of $+0.5$ elementary charges, which is displaced the same distance through the protein dielectric as the H^+-binding site.) The value of the hypothetical charge has been chosen to match the experimental results as follows: if the displacement of $+0.5$ elementary charges is combined with the displacement of the deprotonated H^+-binding site, Asp^{22-} (-1 elementary charges) or the protonated H^+-binding site (uncharged), we obtain net charge displacements of opposite polarity and comparable size dependent on the protonation state of the H^+-binding site (Fig. 7). The $pK_{app} = 8.6$ observed in Fig. 2 *a*, therefore, represents the pK of the H^+-binding site of $GlcP_{Se}$.

Now we can combine the information from the electrical experiments regarding the protonation state of the putative H^+-binding site Asp^{22} (Figs. 2 and 7) with the transport measurements reporting on the pH-independent exchange activity (Fig. 5 *a*), and conclude that sugar is bound, translocated, and released regardless of the protonation state of the putative $GlcP_{Se}$ H^+-binding site. This is a surprising finding for an H^+-coupled symporter that has been shown to support $\Delta\tilde{\mu}_{H^+}$-driven sugar uptake (6).

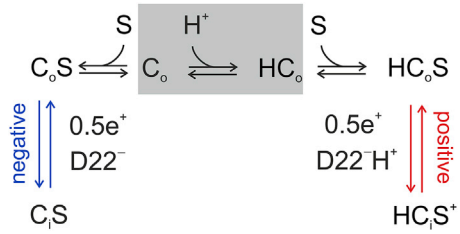

FIGURE 7 Sugar binding to the protonated and unprotonated transporter. The kinetic model shows proton (*shaded region*) and sugar binding to the outward-facing conformation of the transporter C_o, followed by a conformational transition to the inward-facing conformation C_i. In the figure, the final state is represented as an inward-facing conformation C_i because exchange measurements indicate that, independent of pH, sugar is bound, translocated, and released. The H^+-binding residue, Asp^{22} (D22), with or without the proton, is displaced together with a charge localized on the protein of $\sim +0.5$ elementary charges. This results in a positive or negative current, as found experimentally. To see this figure in color, go online.

Sugar/H^+ coupling in $GlcP_{Se}$

The rapidly decaying currents after a sugar concentration jump were identified as pre-steady-state charge displacements (Fig. 1). This demonstrates that $GlcP_{Se}$ driven solely by a glucose concentration gradient does not mediate steady-state electrogenic transport. On the other hand, $GlcP_{Se}$ is capable of sugar exchange (Fig. 5) and sugar transport (6), indicating that under conditions of the electrophysiological assay, glucose moves electroneutrally over the membrane and that $GlcP_{Se}$ is most probably a uniporter.

An interesting behavior of the currents is observed when a pH gradient is applied across the liposomal membrane. When the pH inside the proteoliposomes is higher than that at the outside, that is, the H^+ concentration gradient has the same direction as the applied sugar gradient, the reconstructed electrophysiological currents show a positive steady-state component indicative of continuous turnover (Fig. 4 *b*). Because the only mobile positive charge available for the protein is H^+, it is concluded that H^+ and sugar move in the same direction. This can be considered as a symport-like transport mode. In contrast, when a H^+ concentration gradient is applied in the reverse direction of the sugar gradient, a negative steady-state current component is observed (Fig. 3 *b*). A negative steady-state current indicates the transport of positive charge out of the liposomes when sugar is applied from the outside, giving rise to an antiport-like transport mode.

Regarding the transport directions of sugar and H^+, these transport modes can be considered as sugar/H^+ symport and antiport. However, from a thermodynamic point of view, the picture is more complex. Because the substrates are only loosely coupled, there is no fixed H^+/sugar stoichiometry, and H^+-coupled sugar accumulation is possible only to a minor degree. In fact, both substrates move energetically downhill in both experiments of Fig. 4, although not necessarily in the same direction. At the same time, the sugar and H^+ fluxes are coupled to a certain degree because addition of the sugar induces H^+ flow.

Taken together, these results show that sugar and H^+ fluxes are not completely uncoupled in $GlcP_{Se}$, as may have been inferred from the fact that sugar is translocated irrespective of the protonation of the binding site. This also explains why $\Delta\tilde{\mu}_{H^+}$ stimulates sugar uptake, as previously reported (6). In fact, $\Delta\tilde{\mu}_{H^+}$ stimulated sugar uptake corresponds to the symport-like activity reported above.

Finally, the question arises how bacteria equipped with an only partly coupled H^+/glucose symporter can prevent sugar loss. Sugars, especially glucose, are rapidly metabolized once they enter the cell. Hence, they cannot leave the cell via the same transport process even if uncoupled. Active sugar transport may be an advantage at very low environmental sugar concentrations to increase uptake velocity. However, bacteria of the human commensal microflora, like the host of $GlcP_{Se}$, *S. epidermidis*, most probably face a relatively sugar-rich environment.

$GlcP_{Se}$ as a loosely coupled H^+/sugar transporter

Summarizing, there are clear indications that H^+ and glucose fluxes are coupled in $GlcP_{Se}$, but we also find uncoupled transport modes. The experimental evidence in detail is: 1) D-glucose is bound, translocated, and released in the presence and absence of H^+ in the proton-binding site; 2) experiments in the presence and the absence of a pH gradient demonstrate uniport- as well as partially uncoupled symport- and antiport-like transport modes; and 3) D-glucose affinity is higher in the absence of H^+ in the proton-binding site compared to its presence, indicating that there is no ordered H^+ first/sugar last binding as in other tightly coupled sugar/H^+ symporters. In the following, we will argue that these seemingly contradictory facts may be understood if the requirement of strict substrate coupling is abandoned and $GlcP_{Se}$ is regarded as a loosely coupled transport system. Furthermore, we will demonstrate that a relatively simple kinetic model (Fig. 6) suffices to qualitatively describe the experiments. This is not meant to yield a quantitative comparison with experimental data but instead, a test of whether the inferred phenomena are mechanistically possible and are compatible with the function of the transporter at physiological conditions.

Kinetic models are more than a formal mathematical description of a transport process. A plausible kinetic model implements physico-chemical principles intrinsic to the transport process. Comparison with experimental data, therefore, represents a consistency check for their interpretation. A conventional six-state kinetic model can only describe perfectly coupled transport modes like symport and antiport. However, the universal eight-state model (Fig. 6) can realize any degree of coupling using properly adapted kinetic parameters, and is, therefore, perfect for the description of a loosely coupled transport system.

Our electrophysiological data clearly demonstrate that sugar is bound and translocated with very similar kinetic properties with and without H^+ in the proton-binding site. Therefore, equal rate constants $k = m = 200\ s^{-1}$ are applied in the model. Rate constants n and j have to be significantly smaller to ensure a certain extent of coupling between the sugar and proton fluxes. Here $j = 30$ and $n = 15\ s^{-1}$ are selected accounting for the observation that protonation inhibits the return of the apo transporter (see Results). Overall, these rate constants together with the kinetic parameters given in the legend of Fig. 8 allow for fast sugar binding and translocation as well as turnover rates up to $20\ s^{-1}$, properties similar to those of LacY, a related transporter characterized by comparable current amplitudes (14).

Despite its simplicity and the tentative nature of the kinetic parameters, the model qualitatively reproduces our electrophysiological experiments extremely well. First of all and most interestingly, at symmetrical pH conditions electroneutral sugar transport is found (sugar flux and no H^+ flux,

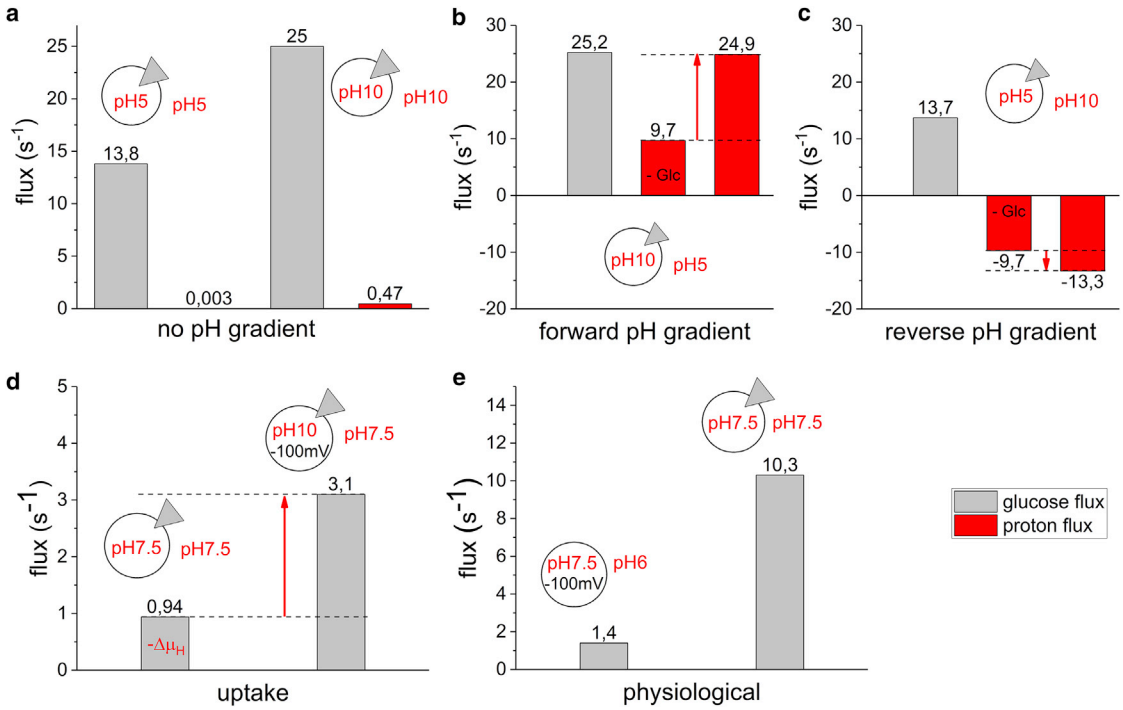

FIGURE 8 Model calculations revealing uncoupled transport modes in a loosely coupled transporter. Simulation of sugar and proton fluxes in an incompletely coupled system are based on the kinetic model of Fig. 6. Kinetic parameters are $j = 30$, $k = 200$, $m = 200$, and $n = 15$. Sugar and proton binding was calculated with $K_D = 3$ mM and pK = 8.6, valence of the binding site $q = -0.5$ elementary charges. (*a*) Simulation of electrophysiological experiments at symmetrical pH. The bars give glucose and proton fluxes after a glucose concentration jump at acidic and alkaline pH. (*b*) Simulation of electrophysiological experiments in the presence of an inward-directed proton concentration gradient. The bars give glucose and proton fluxes after a glucose concentration jump. For comparison, the uncoupled proton flux in absence of glucose is shown (-Glc). The red arrow represents the glucose-stimulated proton flux. (*c*) As in (*b*), but in the presence of an outward-directed proton concentration gradient. (*d*) Sugar transport activity in a typical uptake experiment in the absence ($-\Delta\mu_H$) and presence (*unlabeled bar*) of $\Delta\tilde{\mu}_{H^+}$ (ΔpH = 2.5, $\Delta\psi = -100$ mV). Uptake was calculated at pH 7.5 and 30 μM D-glucose outside. The red arrow represents stimulation of sugar uptake by $\Delta\tilde{\mu}_{H^+}$. (*e*) Comparison of physiological sugar transport in the presence of $\Delta\tilde{\mu}_{H^+}$ (ΔpH = 1.5, $\Delta\psi = -100$ mV, 3 mM D-glucose in- and outside the cell, *left bar*) or a glucose concentration gradient (ΔpH = $\Delta\psi = 0$, 3 mM D-glucose outside the cell, *right bar*). To see this figure in color, go online.

Fig. 8 *a*), representing a uniport-like transport mode. This agrees with the transient currents representing sugar binding, but no steady-state electrical transport, and reflects the loose coupling of sugar and H^+ transport in $GlcP_{Se}$.

At asymmetrical pH conditions, H^+ fluxes follow sugar flux or are opposed to the sugar flux, depending on the pH gradient (Fig. 8, *b* and *c*). The bars labeled "-Glc" represent the uncoupled H^+ leak after application of the pH gradient before the application of the sugar concentration jump, and the unlabeled bars represent the H^+ flux in the presence of the combined sugar/pH gradients after the sugar concentration jump. The difference between the two is the sugar-induced H^+ current (*red arrow*), the quantity determined in the electrophysiological experiments. We also find qualitative agreement with the measurements: a symport-like transport mode in the presence of a driving pH gradient and the antiport-like transport mode in the presence of an oppositely directed pH gradient.

Also, $\Delta\tilde{\mu}_{H^+}$-driven sugar uptake as experimentally demonstrated previously (6) is found with the kinetic model (Fig. 8 *d*). The sugar flux is significantly enhanced (*red arrow*) in the presence of $\Delta\tilde{\mu}_{H^+}$, although coupling is not perfect.

Finally, the model now allows an analysis of the transporter function at physiological conditions (Fig. 8 *e*). *S. epidermidis*, the host organism of GlcP, is part of the normal human skin flora. Typical environmental conditions for the transporter are therefore a mildly acidic external pH (calculations performed with pH 6), a sugar concentration of 1 mM, and a conventional membrane potential of -100 mV. Fig. 8 *e* compares the effect of $\Delta\tilde{\mu}_{H^+}$ (*left bar*) and that of a sugar concentration gradient (*right bar*). Transport is much larger when a sugar concentration gradient is present, indicating that at physiological conditions the residual symport capacity of loosely coupled $GlcP_{Se}$ is irrelevant.

In conclusion, considering that the various reactions in the universal eight-state model can all take place to a certain extent, it seems plausible that different transport modes coexist in a specific transporter if this does not unduly compromise its physiological function. In particular, at in vitro conditions, transport modes may be observable

that are of no importance at physiological conditions. They may, however, give important clues about the mechanism of secondary active transport.

D22N and I105S $GlcP_{Se}$ as models for uniport

$GlcP_{Se}$ mutants mimicking the amino acid configuration in the uniporting GLUT transporters have been proposed as models: D22N and I102S $GlcP_{Se}$ (6). D22N $GlcP_{Se}$ is analogous to the neutral-replacement variants E325A $LacY_{Ec}$, D27N $XylE_{Ec}$, and D46N $FucP_{Ec}$, which show the same phenotype (5,26,27), and like D22N $GlcP_{Se}$, have been qualified as exchange-only variants. In these transporters the negatively charged H^+-binding site is artificially neutralized by a neutral side chain (Asn) rather than by H^+ binding like in the WT. In consequence, sugar transport is uncoupled from $\Delta\tilde{\mu}_{H^+}$ in D22N $GlcP_{Se}$ (6) and pH-independent sugar binding is found (Fig. 2 *c*). Most eukaryotic sugar uniporters, GLUT3, 4, 5, 7, 9, and 11, have this configuration, suggesting that a charged residue in this position is detrimental or irrelevant for uniport.

An exception to this rule is GLUT2, which has a functional H^+-binding site, an Asp in this position, but is a uniporter (1). The analogous model system is I105S $GlcP_{Se}$ which like GLUT2 has a serine in the proximity of the H^+-binding site that has been proposed to interact with the H^+-binding site, thereby precluding symport (6). In the mechanism proposed by Iancu et al. (6), symport in $GlcP_{Se}$ requires the formation of a salt bridge between the unoccupied H^+-binding site Asp^{22} and the conserved Arg^{102} to open the glucose-binding cavity. The salt bridge is subsequently broken by binding of the substrate proton to allow the conformational transition between the inward and outward conformations. In the I105S $GlcP_{Se}$ variant, this mechanism is no longer possible, because Asp^{22} is engaged with Ser^{105}.

We have measured electrogenic sugar binding to the analogous $GlcP_{Se}$ variant, I105S $GlcP_{Se}$, and find a phenotype very similar to WT. It can bind sugar in the protonated and the deprotonated form like WT $GlcP_{Se}$ and its pK_{app} hardly differs from that of WT $GlcP_{Se}$ (8.6 vs. 8.4). This suggests that a serine in position 105 has little effect on H^+ and sugar binding, but more likely exerts its action in a different step of the reaction cycle; for instance, cytoplasmic H^+ release. All the more so, as the interaction of Ser^{105} with Asp^{22} was concluded from an inward-facing structure, from which H^+ release is expected to take place.

In the light of our data, we have to assume that WT $GlcP_{Se}$ is a loosely coupled transporter. The fact that I105S $GlcP_{Se}$ does not respond to $\Delta\tilde{\mu}H^+$ (6) suggests that in this variant coupling is further reduced, transforming it essentially into a uniporter. The mechanism by which this is accomplished involves Asp^{22} and Arg^{102}; interestingly, homologous residues to Asp^{27} and Arg^{133} in $XylE_{Ec}$ have been implicated in a pK-switch (together with Glu^{206}) (7). We, therefore, may envision the alternative possibility that a disabled pK switch preventing effective H^+ release brings about the phenotype of the I105S variant. This would lead to

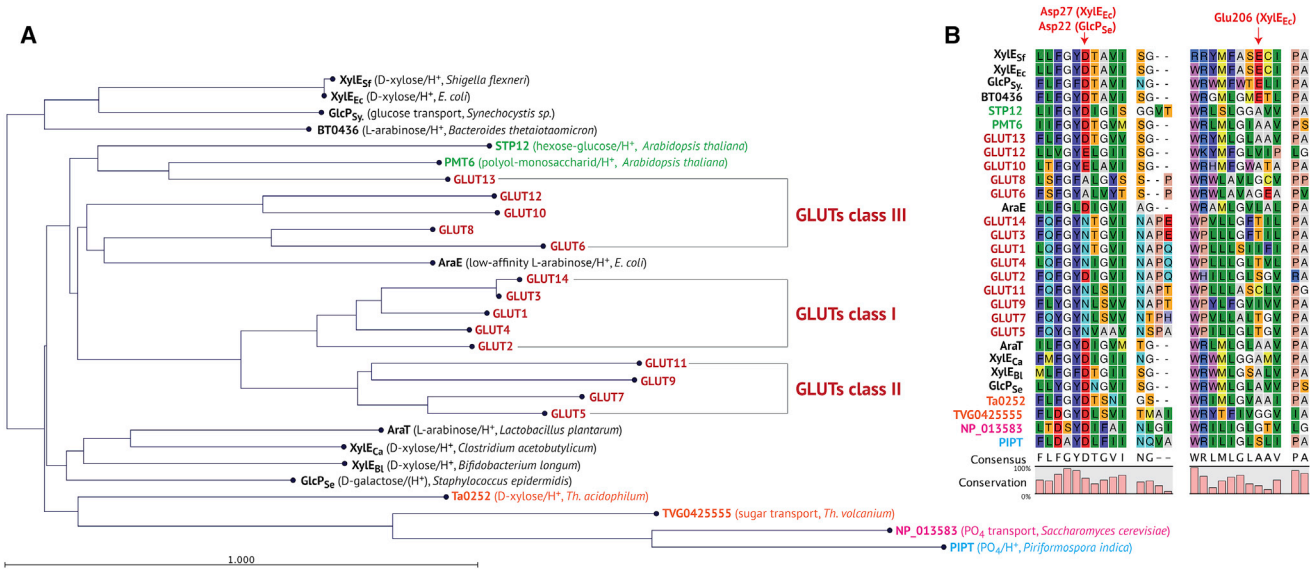

FIGURE 9 Phylogenetic similarity of selected MFS transporters. (*A*) Similarity between the transporters is illustrated as a phylogenetic tree. It is constructed using the Neighbor Joining Method and the Kimura distance matrix. The bar (*lower left*) indicates the scale of evolutionary divergence between two nodes (1/100 nucleotides). (Color code: *red*, animals; *green*, plants; *magenta*, yeast; *blue*, fungi; *black*, bacteria; *orange*, archaea.) (*B*) Amino acid sequences alignments showing the vicinity of the H^+-binding site (Asp^{27} in $XylE_{Ec}$ and Asp^{22} in $GlcP_{Se}$) and the putative coupling residue (E206 in $XylE_{Ec}$). The sequence alignments and the phylogenetic tree were generated using the CLC Sequence Viewer (V. 7.7; Qiagen Bioinformatics, https://www.qiagen.com/us/). To see this figure in color, go online.

recycling of the substrate proton accounting for the lack of stimulation by $\Delta\tilde{\mu}_{H^+}$ (6).

Symport needs more than a H^+-binding site

In conclusion, the model calculations in agreement with our experimental studies demonstrate that H^+/sugar coupling is incomplete in $GlcP_{Se}$ leading to the unexpected finding that depending on the experimental conditions $GlcP_{Se}$ can function as a symporter, or show partially uncoupled transport modes. However, at physiological conditions, $GlcP_{Se}$ predominantly operates as a uniporter driven by an inward-directed sugar gradient. This raises the question why this transporter has a functional H^+-binding site. In comparison, most human GLUT sugar transporters, homologs of GlcP, have lost the H^+-binding site and their symport capacity, probably due to the availability of relatively high sugar concentrations in their environment (6). The same argument, high environmental sugar concentrations, is also possibly valid for $GlcP_{Se}$ and the habitat of its host, *S. epidermidis*. Therefore, $GlcP_{Se}$ may be an evolutionary intermediate form of a sugar transporter, which has lost most of its sugar/H^+ symport capacity but still has a functional H^+-binding site as a relic of its prokaryotic origin.

A comparison based on phylogenetic similarity of a number of MFS transporters related to $GlcP_{Se}$ is shown in Fig. 9 *A*. The bacterial transporters (*black* in Fig. 9 *A*) group in two clusters: one that comprises $XylE_{Ec}$, a tightly coupled H^+/sugar symporter; and one that comprises $GlcP_{Se}$, a loosely coupled sugar transporter. The analysis reveals also that the large cluster of eukaryotic sugar transporters (GLUTs Class I, II, III, and the *Arabidopsis thaliana* sugar transporters) is closer related to the transporters that cluster with $GlcP_{Se}$. However, recent studies have shown a higher conservation of the sugar-binding residues of GLUT1 in $XylE_{Ec}$ compared to $GlcP_{Se}$ (5). All bacterial transporters harbor a H^+-binding site, Asp^{27} in $XylE_{Ec}$ or Asp^{22} in $GlcP_{Se}$ (Fig. 9 *B*). In contrast, some of the eukaryotic sugar transporters have a H^+-binding site (e.g., GLUT2 and GLUT10; Fig. 9 *B*), some have none (e.g., GLUT1 and GLUT5). This seems to suggest that transporters with a H^+-binding site are H^+/sugar symporters and transporters without one are uniporters. However, some transporters possessing a H^+-binding site were reported to be uniporters (GLUT2 (1)) or to be only incompletely coupled ($GlcP_{Se}$). Therefore, it has been proposed that the existence of a H^+-binding site is a necessary but not a sufficient requirement for H^+/sugar symport (6). This raises the question what could be the additional structural element for strictly coupled transport. In a previous publication, it was hypothesized that the glutamate at position 206 in $XylE_{Ec}$ is a residue critically involved in the pK-switch of the H^+-binding site to acidic values to facilitate H^+ release (7). Interestingly, the bacterial transporters in the $XylE_{Ec}$ cluster all have this residue. We, therefore, propose that for tight coupling a pK switching residue like Glu^{206} in $XylE_{Ec}$ is required in addition to a H^+-binding site and that in its absence, as is the case in the $GlcP_{Se}$ cluster, coupling is incomplete. Because all eukaryotic transporters have an uncharged residue in the corresponding position, we predict that they are only incompletely coupled even if they possess a H^+-binding residue like GLUT2 and GLUT10, 12, and 13. This may explain why some of these transporters have been classified as uniporters (GLUT2 (1)) others as symporters (GLUT12 (4), GLUT13 (1)). Mutational studies of E206 in $XylE_{Ec}$ and A167 in $GlcP_{Se}$ are planned to identify the requirements for strict coupling in MFS sugar/H^+ symporters.

SUPPORTING MATERIAL

Supporting Materials and Methods and one figure are available at http://www.biophysj.org/biophysj/supplemental/S0006-3495(17)31119-0.

AUTHOR CONTRIBUTIONS

A.B. designed research, performed research, analyzed data, and wrote the article. A.J.Z. performed research and analyzed data. A.S. performed research and analyzed data. M.G.M. analyzed data and wrote the article. K.F. initiated and designed research, analyzed data, and wrote the article.

ACKNOWLEDGMENTS

The plasmid pET15b with the WT $GlcP_{Se}$ construct was a generous gift of Jun-Yong Choe (The Chicago Medical School, Rosalind Franklin University of Medicine and Science, Chicago). We are also indebted to Jun-Yong for critical reading of the manuscript and helpful discussions. We thank Lina Hatahet for excellent technical assistance.

This study was supported by the Deutsche Forschungsgemeinschaft, SFB 807 (to K.F.). K.F., A.B., and A.J.Z. gratefully acknowledge continuous support of the project by Ernst Bamberg (Max Planck Institute of Biophysics, Frankfurt, Germany).

REFERENCES

1. Mueckler, M., and B. Thorens. 2013. The SLC2 (GLUT) family of membrane transporters. *Mol. Aspects Med.* 34:121–138.
2. Uldry, M., and B. Thorens. 2004. The SLC2 family of facilitated hexose and polyol transporters. *Pflugers Arch.* 447:480–489.
3. Pujol-Giménez, J., A. Pérez, …, M. P. Lostao. 2015. Functional characterization of the human facilitative glucose transporter 12 (GLUT12) by electrophysiological methods. *Am. J. Physiol. Cell Physiol.* 308:C1008–C1022.
4. Wilson-O'Brien, A. L., N. Patron, and S. Rogers. 2010. Evolutionary ancestry and novel functions of the mammalian glucose transporter (GLUT) family. *BMC Evol. Biol.* 10:152.
5. Madej, M. G., L. Sun, …, H. R. Kaback. 2014. Functional architecture of MFS D-glucose transporters. *Proc. Natl. Acad. Sci. USA.* 111:E719–E727.
6. Iancu, C. V., J. Zamoon, …, J. Y. Choe. 2013. Crystal structure of a glucose/H^+ symporter and its mechanism of action. *Proc. Natl. Acad. Sci. USA.* 110:17862–17867.
7. Bazzone, A., M. G. Madej, …, K. Fendler. 2016. pH regulation of electrogenic sugar/H^+ symport in MFS sugar permeases. *PLoS One.* 11:e0156392.

8. Bazzone, A., W. S. Costa, …, K. Fendler. 2013. Introduction to solid supported membrane-based electrophysiology. *J. Vis. Exp.* 75:e50230.
9. Schulz, P., J. J. Garcia-Celma, and K. Fendler. 2008. SSM-based electrophysiology. *Methods.* 46:97–103.
10. Bazzone, A., M. Barthmes, and K. Fendler. 2017. Chapter two - SSM-based electrophysiology for transporter research. *In* Methods in Enzymology. C. Ziegler, ed. Academic Press, Cambridge, MA, pp. 31–83.
11. Garcia-Celma, J. J., B. Dueck, …, K. Fendler. 2008. Rapid activation of the melibiose permease MelB immobilized on a solid-supported membrane. *Langmuir.* 24:8119–8126.
12. Mager, T., A. Rimon, …, K. Fendler. 2011. Transport mechanism and pH regulation of the Na^+/H^+ antiporter NhaA from *Escherichia coli*: an electrophysiological study. *J. Biol. Chem.* 286:23570–23581.
13. Garcia-Celma, J. J., I. N. Smirnova, …, K. Fendler. 2009. Electrophysiological characterization of LacY. *Proc. Natl. Acad. Sci. USA.* 106:7373–7378.
14. Garcia-Celma, J. J., J. Ploch, …, K. Fendler. 2010. Delineating electrogenic reactions during lactose/H^+ symport. *Biochemistry.* 49:6115–6121.
15. Gaiko, O., A. Bazzone, …, H. R. Kaback. 2013. Electrophysiological characterization of uncoupled mutants of LacY. *Biochemistry.* 52:8261–8266.
16. Meyer-Lipp, K., C. Ganea, …, K. Fendler. 2004. Sugar binding induced charge translocation in the melibiose permease from *Escherichia coli*. *Biochemistry.* 43:12606–12613.
17. Gropp, T., F. Cornelius, and K. Fendler. 1998. K^+-dependence of electrogenic transport by the Nak-ATPase. *BBABiomembr.* 1368:184–200.
18. Borlinghaus, R., H. J. Apell, and P. Läuger. 1987. Fast charge translocations associated with partial reactions of the Na,K-pump: I. current and voltage transients after photochemical release of ATP. *J. Membr. Biol.* 97:161–178.
19. Tadini-Buoninsegni, F., and K. Fendler. 2015. Recording of pump and transporter activity using solid-supported membranes (SSM-based electrophysiology). *In* Pumps, Channels and Transporters: Methods of Functional Analysis. R. J. Ronald, J. Clarke, and M. A. Ali Khalid, eds. Wiley, Hoboken, NJ, pp. 147–177.
20. Viitanen, P., M. L. Garcia, …, H. R. Kaback. 1983. Mechanism of lactose translocation in proteoliposomes reconstituted with Lac carrier protein purified from *Escherichia coli*. 2. Deuterium solvent isotope effects. *Biochemistry.* 22:2531–2536.
21. Smirnova, I. N., V. Kasho, and H. R. Kaback. 2008. Protonation and sugar binding to LacY. *Proc. Natl. Acad. Sci. USA.* 105:8896–8901.
22. Heinz, E. 1989. The unfinished story of secondary active transport. *In* Membrane Transport, People and Ideas. D. C. Tosteson, ed. American Physiological Society, Bethesda, MD, pp. 237–250.
23. Heinz, E., P. Geck, and W. Wilbrandt. 1972. Coupling in secondary active transport. Activation of transport by co-transport and-or counter-transport with the fluxes of other solutes. *Biochim. Biophys. Acta.* 255:442–461.
24. Adelman, J. L., C. Ghezzi, …, M. Grabe. 2016. Stochastic steps in secondary active sugar transport. *Proc. Natl. Acad. Sci. USA.* 113:E3960–E3966.
25. Schuldiner, S. 2014. Competition as a way of life for H^+-coupled antiporters. *J. Mol. Biol.* 426:2539–2546.
26. Carrasco, N., I. B. Püttner, …, H. R. Kaback. 1989. Characterization of site-directed mutants in the Lac permease of *Escherichia coli*. 2. Glutamate-325 replacements. *Biochemistry.* 28:2533–2539.
27. Dang, S., L. Sun, …, N. Yan. 2010. Structure of a fucose transporter in an outward-open conformation. *Nature.* 467:734–738.